Vibration-based damage identification with application to a scaled masonry arch

Daniele Brigante[a], Maria Giovanna Masciotta[b], Carlo Rainieri[a], Giovanni Fabbrocino[a,c], Paulo B. Lourenço[b]
[a] *University of Molise, StreGa Lab, DiBT Department, Via Francesco De Sanctis, 86100 Campobasso, Italy*
[b] *ISISE, University of Minho, Department of Civil Engineering, Guimarães, Portugal*
[c] *ITC-CNR. Construction Technologies Institute, National Research Council of Italy (CNR), L'Aquila Branch, Via Carducci, L'Aquila, Italy*

Keywords: Dynamic testing, Damage assessment, Vibration based methods, Masonry arch, Modal identification.

ABSTRACT
Remote and automated evaluation of the structural health conditions of structures may play a primary role in management and planning of appropriate maintenance interventions, avoiding downtime and expensive interventions due to significant degradation and damage progression. In order to timely detect emerging damage conditions, dynamic identification procedures and vibration-based structural health monitoring can be applied.
The present paper describes the main outcomes of an experimental study aimed at assessing the relationship between controlled damage conditions and changes in dynamic properties of the structure under consideration. Tests have been carried out on a scaled replica of an ancient masonry arch, which was subjected to multiple damage scenarios characterized by increasing levels of horizontal settlements of one of the abutments.
Damage detection has been carried by means of a spectrum driven damage identification method, whose capacity to support health condition diagnosis of the arch has been investigated. Despite the complex experimental process, encouraging results were obtained, demonstrating a certain ability of damage detection process to support health stated evaluations of masonry arches. Further work and more detailed analyses are needed to point out critical features of the procedure and define strategies for improving accuracy and reliability.

1 INTRODUCTION

Protection of architectural heritage may be achieved by means of proper assessment of current conditions through a path of knowledge (Rainieri et al., 2015a) and computational models (Lourenço, 2002); so doing upgrading interventions compliant with conservation criteria can be also designed (ICOMOS, 2003). However, this is not the only way to preserve heritage and existing constructions, since development of technology and sensors offer advanced tools for the timely detection of anomalies even in the case of exceptional events either due to natural (Ferreira et al., 2019; Miranda and Ferreira, 2019) or anthropic hazards (Granda & Ferreira, 2019), which have seriously affected the cultural heritage in recent years. Vibration-based damage identification methods (VBDIMs) in such a context can play a relevant role in combination with reliable procedures able to provide continuous extraction of relevant parameters from the measures (Rainieri and Fabbrocino, 2015b), so that the structural condition of non-conventional systems and the onset of damage can be detected at the earliest possible stage (Masciotta et al. 2016a). This approach to the condition assessment of heritage construction can contribute to the definition of cost-effective and reliable maintenance and restoration processes, since the early detection and the definition of the evolution in time of undesired phenomena improve the design of countermeasures and the overall safety conditions of architectural complexes and heritage urban areas (Marra et al., 2019). In the framework of the work illustrated in the present paper, damage is assumed to be as an adverse condition that jeopardises the structural integrity of a system and affects its performance in terms of load-bearing capacity of the structural elements, materials strength and stiffness. The alterations induced into the system by the damage and the reversibility of the process depend on the

severity and size of the damage and last, but not the least, on the number and type of elements involved. The stiffness degradation due to the loss of structural integrity will be reflected in changes of the properties of the system in terms of modal parameters (frequencies, mode shapes and damping ratios).

The possibility to easily measure these quantities has been fostering their use as damage indicators in all engineering fields (Wahab & De Roeck, 1999). Dynamic tests under environmental excitations, in conjunction with model updating techniques (Masciotta et al., 2016b) represent an effective non-destructive tool for the assessment of the dynamic behaviour of existing and, in particular, historical constructions. It is worth noting that numerical modelling by the finite element method (FEM) may play a relevant role in the development of effective damage detection monitoring systems, since it is able to support the design of the vibration based monitoring systems, as well as to guide the assessment of the structural performance once an optimised model is achieved (Rainieri et al., 2013).

This is the background of the present paper that reports the main outcomes of an experimental campaign carried out on a scaled masonry arch replica at the Structural Lab of the University of Minho in Guimarães (Portugal). Attention is paid to the design and the implementation of the tests and to the interpretation and analysis of the measures for damage detection purposes by means of the spectral-based algorithm (Ramos et al. 2010, Masciotta, 2016a). Damage was induced on the specimen by a mechanical actuator under displacement control. In the next sections, the main aspects of the test design and relevant results are reported along with some concluding remarks.

2 ARCH MODEL DESCRIPTION AND NUMERICAL SIMULATIONS FOR TEST DESIGN

A set of scaled replicas of ancient masonry arch were built in a semi-circular shape with a radial thickness of 75 mm, 1900 mm span, 430 mm and springing angle of 40° (Figure 1).

They were made of low compressive strength clay bricks from the Northern area of Portugal assembled with staggered lime mortar joints (approximately 5 mm thick); low strength mortar was used to fit characteristics of historical constructions.

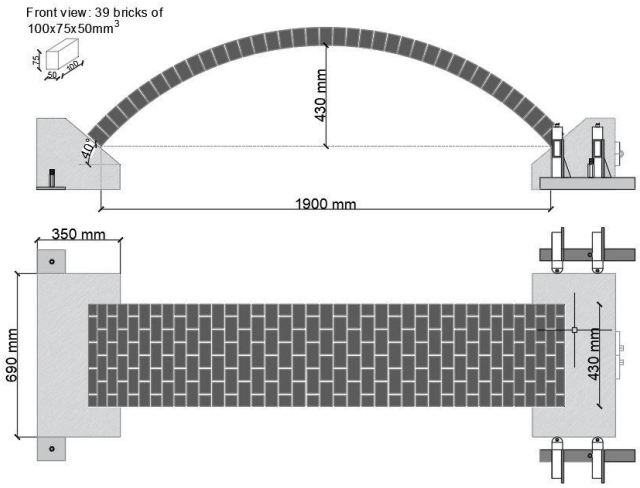

Figure 1. Arch geometry.

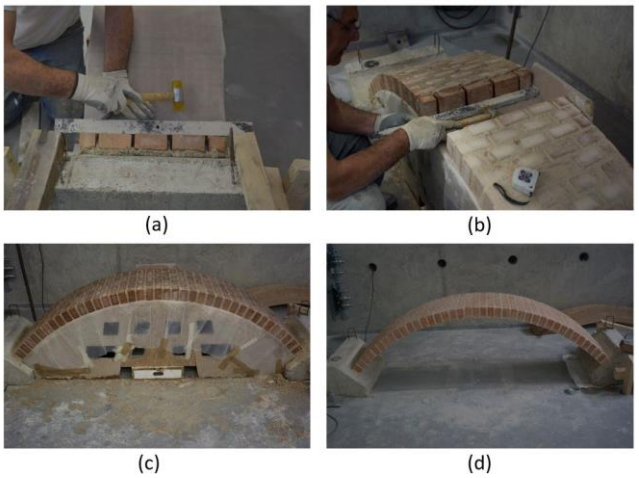

Figure 2. Arch model build: a) starting construction; b) ending phase; c) demoulding; d) arch completed.

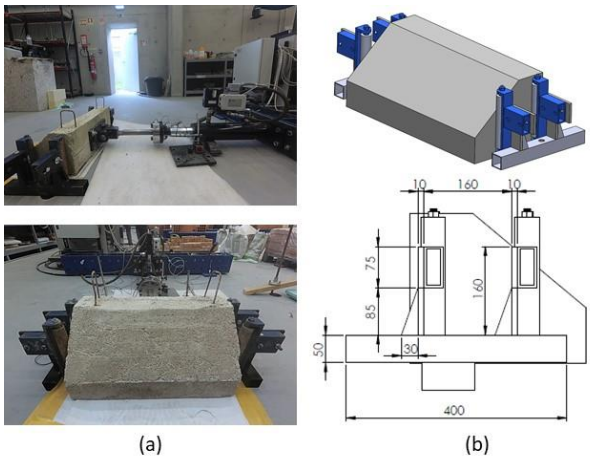

Figure 3 View of the loading (a) and rolls system (b).

The abutments were made of concrete over rectangular steel plates fixed to the laboratory floor. The arches were built, over a wooden mould keeping a constant intrados mortar joint thickness of 5 mm and 10 mm near the abutments. The demoulding process was made after one week; Figure 2 shows the main phases of the arch construction.

The experimental tests were aimed at measuring the dynamic response of the arch when subjected to given value of the relative displacement of the abutments. To this end, the left abutment was fixed to the floor, while the right one was guided to slide on a Teflon sheet in the longitudinal direction (Figure 3).

2.1 Design numerical model

The design of the tests was carried out by using a numerical analysis of the specimens. A Finite Element (FE) model was developed in the software DIANA Ver. 10.2, so that linear and non-linear analyses could be carried out. As FE linear analyses are concerned, the results of modal analyses were used to optimise the sensor layout and the measurement chain in terms of sensor specifications and sampling frequency. As above already mentioned, the arch was composed of full brick masonry units (A) and lime mortar. The range of variation of material characteristics was chosen referring to data provided by the Italian Code and specific available data (Basilio, 2007).

Table 1. Mechanical properties of the masonry arch model

Masonry typology	fm [MPa]	τ_0 [MPa]	E [MPa]	G [MPa]	W [kNm^{-3}]
	min max	min max	min max	min max	-
A	2.40 4.00	0.06 0.092	1200 1800	400 600	18

Linear softening in tension and parabolic softening in compression were selected, as shown in Figure 4. They depend on the selection of an appropriate value of the fracture energy both in tension, G^I_f - set equal to 0,015 N/mm, being h equal to 0,029 mm, and in compression, G_c - set equal to 9,60 N/mm being h equal to 2,4 mm - (Feenstra, 1993; Lourenço, 2009).

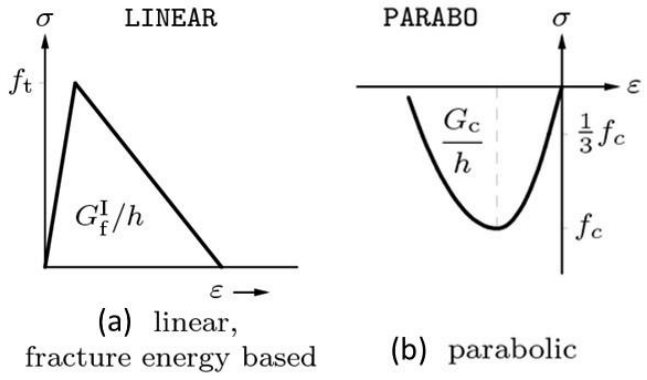

Figure 4. Arch 3D model: tensile (a) and compressive (b) behaviour

A macro-modelling approach (Lourenço 2009) was used, so that bricks, mortar and brick–mortar interface is smeared out in a homogeneous continuum. The constitutive model based on total strain rotating crack is implemented for the FE model, this approach is improved along the bases of the Modified Compression Field Theory, originally proposed by (Bentz, et al. 2006).

The reference value reported in Table 1 are adopted for characterizing the mechanical property of the model, in particular, Young modulus of 1800 MPa, Poisson coefficient equal to 0.2, mass density equal to 18 kN/m^3. The concrete abutments were assumed linear elastic with a Young's modulus equal to 30000 MPa, the Poisson coefficient equal to 0.2, mass density equal to 25 kN/m^3 were assumed for the analysis.

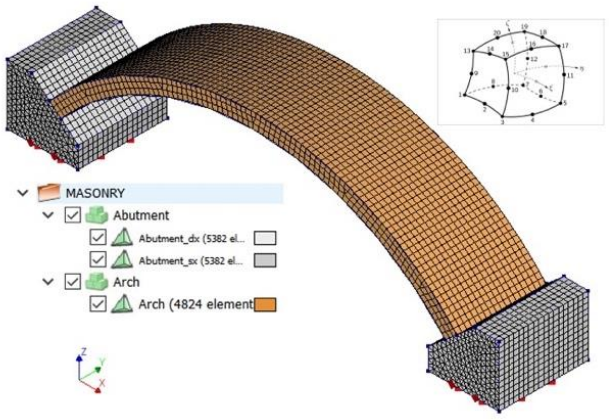

Figure 5. 3D FE model: view of the mesh type and the boundary conditions for the modal analysis.

The Finite Element Model (FEM) of the arch (Figure 5), reproduces in detail the geometry of the specimens. Solid brick elements CHX60 were adopted for this numerical model. This is a twenty-node isoparametric solid brick element and is based on Gauss integration and quadratic interpolation. These elements, for the reference scenario (RS), are characterized at the base by perfect constraints.

The arch solid part has been generated in continuity with the surface of the abutments. An average size QUAD element was considered in the optimized mesh of all the components. The first stage of the analysis, obviously, started with the 3D undamaged model, assumed as reference for further analyses on the deformed/loaded arch.

2.1.1 Modal Dynamic Analysis

The free vibration eigenvalue analysis that is made available by DIANA solver was performed. A modal dynamic analysis was carried out on the arch model. Figure 6 shows the results in terms of

frequency values and mode shape configurations for the first six modes. Consequently, it was expected to define experimentally, at least, six distinct frequencies.

The bandwidth of the relevant mode shapes was identified; the first natural frequency was found to be about 35 Hz, while the sixth one was found to be about 120 Hz. The review of both natural frequencies and mode shapes collected in Figure 6 confirmed the absence of close modes and an upright distribution of the modes in the abovementioned bandwidth.

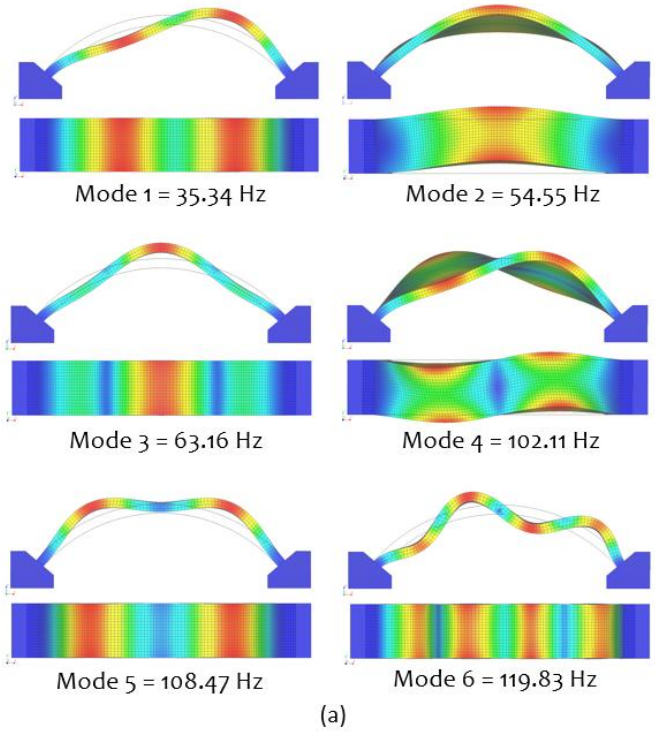

Figure 6. Numerical modal results: front and top view.

2.1.2 Simulation of damage

The FE model has been then subjected to an increasing displacement load to predict the possible location of damage. The load process was governed by an imposed displacement at the base of the right abutment base (Figure 7), in compliance with the real configuration of the specimen.

Increase of the displacement was made by using a step of 0.1 mm until the conventional collapse assumed at the last step characterized by a numerical convergence, for sake of simplicity.

On this subject, it is worth noting that the simulation of the full development of the collapse mechanism was out of the scope of the analysis, being attention focussed on the location of crack location and on the estimation of the damaged zone. For the static response the analyses show three cracks (hinges) at ultimate load step (Figure 8).

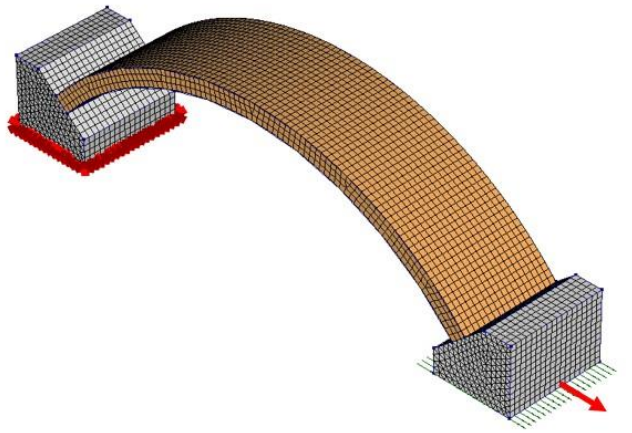

Figure 7 View of the sliding boundary conditions for the right abutment.

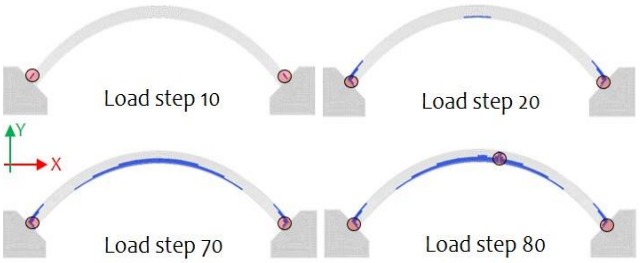

Figure 8. Main crack sequence from the predictive model.

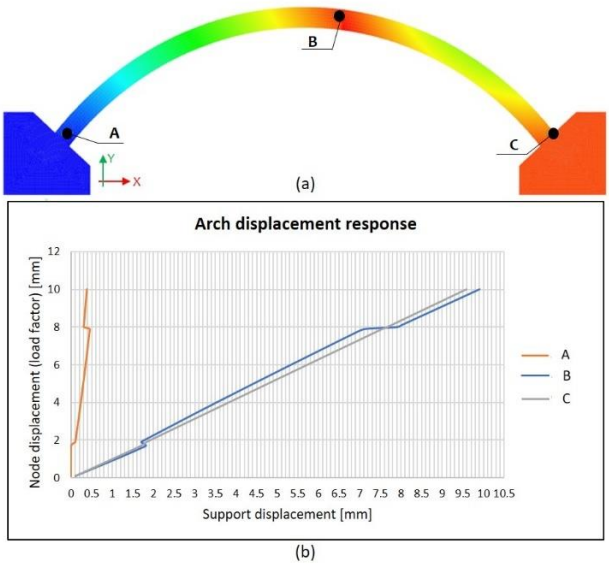

Figure 9. Numerical simulation: a) view of the control point; b) displacement of the control points.

For the prediction model, the crack sequence shows that the first two cracks appear simultaneously in the extrados in a symmetrical position close to the supports with a displacement of the support equal to 1.6 mm.

The third and last crack appear in the intrados close to the crown position on the right side for a displacement equal to 8 mm. The total displacement associated with the incremental load step has been plotted in Figure 9b. Assuming that

the interface between the support and the arch is not completely broken, the result shows a higher similarity of the displacements for the control points B and C compared to control point A.

3 EXPERIMENTAL TESTS

3.1 Static loading of the arch

Experimental tests consisted in a series of seven static loading steps and consequent dynamic measurements of the environmental vibrations of the arch. Figure 10 provides a view of the specimen during testing. The measures of the relative displacements between the abutments were taken by means of the LVDTs arranged as represented in Figure 10a.

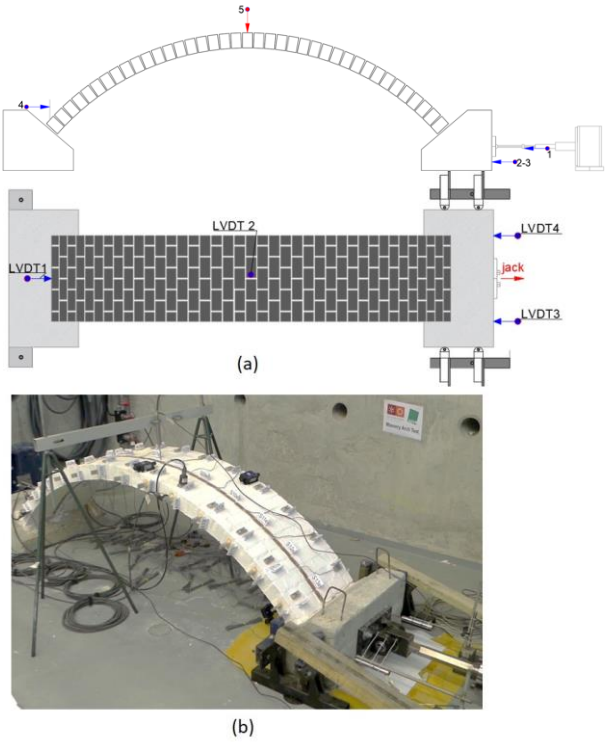

Figure 10. Arch test: a) LVDT layout; b) view of the apparatus.

Two additional LVDTs were installed in order to measure the displacement of the actuator, the last one was placed to measure the vertical displacement of the arch key. As the static response of the arch is concerned, it was observed a general agreement between the predicted response of the system and the experimental one.

Expected cracks became clearly visible from the third Damage State (DS) – DS_{III}, displacement equal to 1.6 mm -. Figure 11 provides a view of the cracks, identified by numbered tags. Cracks C1 and C3 appeared at an early stage during the second damage state application, DS_{II} with a displacement of 1.0 mm.

Crack C2 appeared first at the left side of the crown, then involved all the cross section at the last damage scenario DS_{VII}, displacement equal to 3.7 mm.

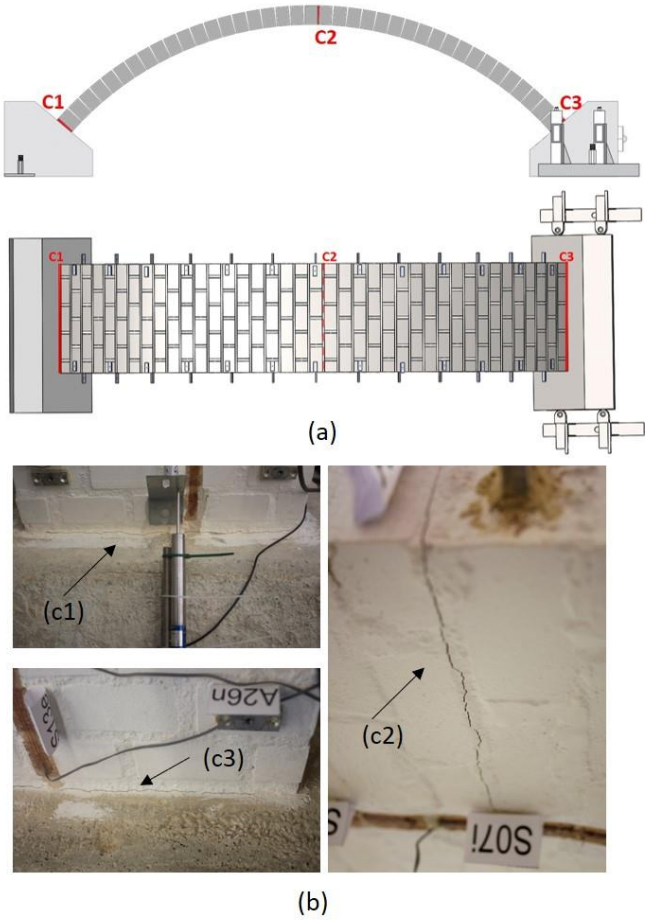

Figure 11. Arch damage: a) view of crack location; b) crack C1, C2 and C3.

3.2 Dynamic identification of the arch

Dynamic identification tests were carried out at each static loading step by means of the recording of the response of the arch under environmental vibrations. Piezoelectric mono-directional accelerometers with nominal sensitivity of 1000 mV/g, frequency interval (±5%) from 0.15 to 1000 Hz (5%), 8 μg of resolution and 210 g of weight, were used.

The sensor layout is represented in Figure 12; it was defined based on the results of the numerical analysis, which demonstrated that the majority of relevant mode shapes were characterised by deformation in the vertical direction and only the second and the fifth mode exhibited displacement in the transverse – horizontal – direction. Based on these results and in relation with the type of imposed loads, the sensors were installed in the normal and tangent direction to the curved

surface of the arch.

Observability of torsional modes of the arch cross section was pursued by installing the sensors in the proximity of the front and back edges of the arch. A number of 13 measurement points evenly spaced for both edges of the arch were marked. The accelerometers were attached by screws to aluminium plates and then directly glued to the arch. As a secondary sensor layout, fourteen strain gauges (series PL-120-11) were installed along the extrados and intrados middle line; they were used to measure the strain distribution and also to investigate the capacity of these sensors of providing dynamic measures to be used in damage detection techniques. For sake of brevity, in the following reference is made only to the measures taken from the piezoelectric accelerometers.

Table 2. Test setups for accelerometers, n = normal direction and t = tangential direction.

	Ch1,2	Ch3,4	Ch5	Ch6	Ch7	Ch8
Setup	Reference sensors		Rolling sensors			
	1.n, t	2.n, t	1.n	2.t	3.n	4. t
1	A09	A18	A01	A01	A14	A14
2	A09	A18	A02	A02	A15	A15
3	A09	A18	A03	A03	A16	A16
4	A09	A18	A04	A04	A17	A17
5	A09	A18	A05	A05	A19	A19
6	A09	A18	A06	A06	A20t	A20
7	A09	A18	A07	A07	A21t	A21
8	A09	A18	A08	A08	A22t	A22
9	A09	A18	A10	A10	A23t	A23
10	A09	A18	A11	A11	A24t	A24
11	A09	A18	A12	A12	A25t	A25
12	A09	A18	A13	A13	A26t	A26

A fine resolution in the modal estimation was pursued by defining 52 recorded degrees of freedom (26 in the normal direction and 26 in the tangential direction) according to the scheme provided Figure 12a. Due to the availability of eight sensors, 12 layouts with four reference sensors in positions A09 and A18 and 4 rolling sensors were placed in the front and back edges; Table 2 summarizes the sequential process. This resolution is really fine in a laboratory environment and supports a good to definition of the mode estimates, but it is clear that from a practical point of view that, too many points are unpractical and expensive for experimental tests in real structures.

Data acquisition (Figure 13) of the accelerometer measurements was carried out by a measurement device with 16 bit resolution and on-board anti-aliasing filter. The data acquisition hardware is managed by a software developed in LabView environment. The signals from the accelerometric sensors were sampled at a frequency of 400 Hz per channel; a minimum measuring time of 60 s for the random impact and 180 s for the ambient excitations were selected in order to achieve a sustainable duration of the entire loading process and avoid influence on the results of the non-linear phenomena activated in the hinge regions.

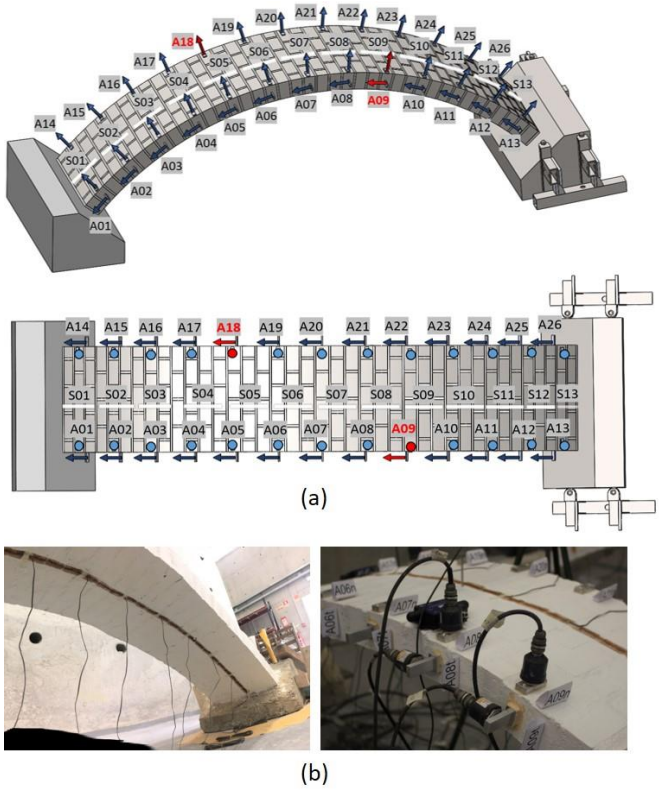

Figure 12. a) Location of the measuring points for the dynamic tests: a) front and top view. *Ai* indicates accelerometers and *Si* indicates strain gauges; b) view of the dynamic apparatus.

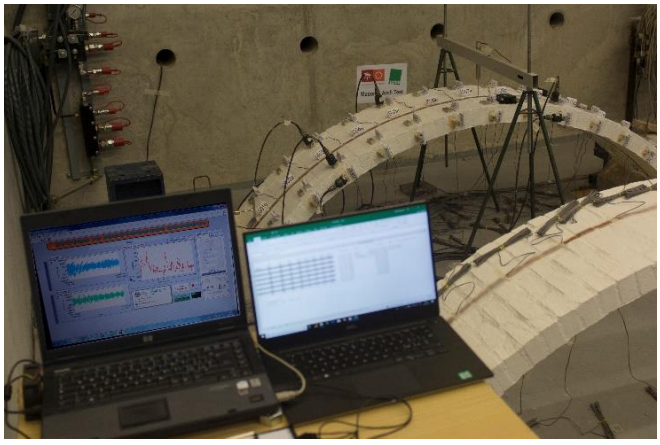

Figure 13. Data acquisition system.

3.2.1 Modal properties and damage evolution

The acquired data were analysed with two different methods: the FDD and the SSI-Principal

Component available in ARTeMIS software (SVS, 2018), obtaining the estimation of a significant number of modes; attention herein is focussed on five of them in the bandwidth 30–160 Hz. Actually, the specific laboratory environment was rather hard for the dynamic identification due to a low vibration level and at the same time to the presence of mechanical devices under operation. So herein for the sake of brevity, the results collected in Table 3, and 4 and Figure 14 refer to random impact tests.
In particular, Table 3 shows the comparison made by using the MAC matrix between the results obtained from EFDD and SSI-PC procedures. The MAC index is generally high, greater than 0.9, except for Mode 3 (in the DS_V).

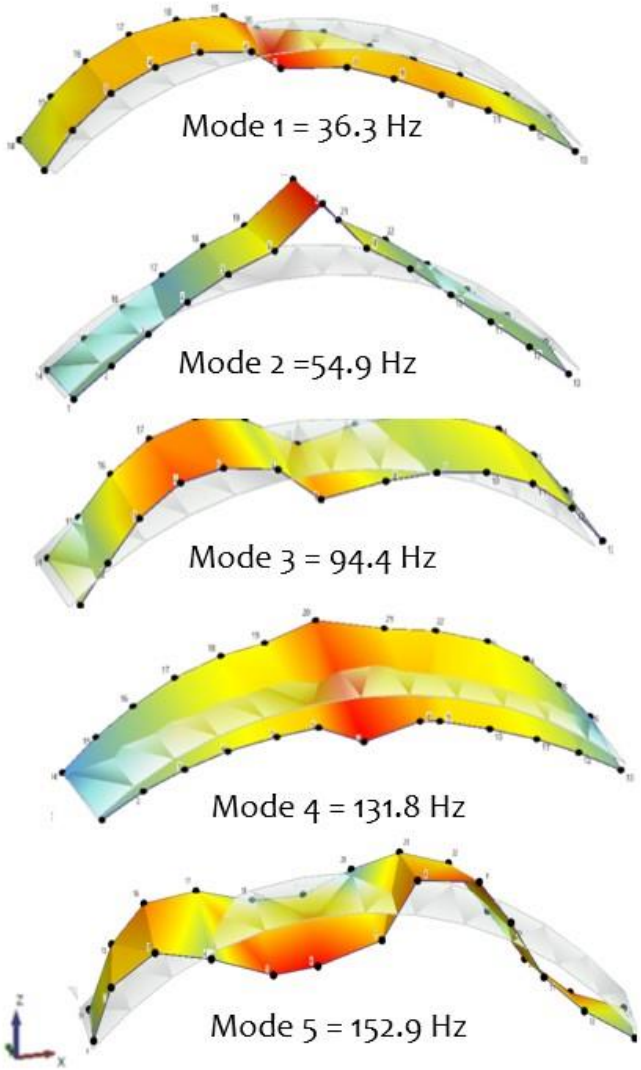

Figure 14. Experimental modal shapes of the undamaged (RS) arch configuration from SSI-PC of random impact test measures.

Table 4, instead, provides an overview of the natural frequencies depending on the level of damage induced on the arch; the table shows the detailed correspondence between the generic conventional Damage State, DS, and the Imposed Displacement (ID). The five identified mode shapes for the undamaged condition are shown in Figure 14.

Table 3. EFDD-SSI-PC MAC matrix - random impact test.

Mode #1	Mode #2	Mode #3	Mode #4	Mode #5
1.00	1.00	0.99	0.99	0.67
1.00	1.00	0.91	0.97	0.55
1.00	1.00	0.98	0.92	0.92
1.00	1.00	0.99	1.00	0.93
1.00	1.00	0.98	1.00	0.85
1.00	1.00	0.98	1.00	0.92
1.00	1.00	0.74	1.00	0.93
1.00	1.00	0.95	0.99	0.94

Table 4. SSI-PC results from random impact test

DS	ID	Frequency ω [Hz] of the Mode				
	[mm]	# 1	# 2	# 3	# 4	# 5
REF	0.0	36.3	54.9	94.4	131.8	152.9
I	0.6	33.2	51.3	84.0	128.5	149.4
II	1.0	32.0	50.1	82.5	118.1	144.4
III	1.6	30.4	48.4	80.3	125.1	138.5
IV	2.1	29.6	47.8	79.1	123.7	135.0
V	2.7	29.2	47.4	78.9	123.5	134.0
VI	3.1	28.7	47.0	78.0	122.0	132.6
VII	3.7	28.6	46.5	77.4	122.0	132.6

4 SPECTRUM DRIVEN DAMAGE IDENTIFICATION METHOD

The extraction of the modal parameters of the masonry arch is the first phase of a damage detection procedure. In this section, attention is devoted to the spectrum driven damage identification methods, whose ability to provide reliable results is checked against the experimental test results. Before going into the details of the present application, a brief recall of the methodology is proposed.

4.1 Basics of the methodology

In stochastic environment, the response X(t) of a system to dynamic loading F(t) can be defined as unidimensional multivariate stochastic vector process, whose elements are the time-dependent nodal response processes. In this context, the dynamic characterisation of a given structural system can be performed by the use of normal spectral analysis methods based on the eigenvalue decomposition of the Power Spectral Density (PSD response matrix according to the following equation:

$$S_x(\omega) = \Psi_X(\omega)\Lambda_X(\omega)\Psi_X^H(\omega) \quad (1)$$

Where $\Lambda_X(\omega)$ is a diagonal matrix containing frequency-dependent ordered eigenvalues:

$$\Lambda_X(\omega) = diag\{\lambda_1(\omega),..\lambda_j(\omega),..\lambda_i(\omega)\} \quad (2)$$

while $\Psi_X(\omega)$ is a complex matrix including mutually orthogonal eigenvectors as columns and $\Psi_X^H(\omega)$ denotes the conjugate transpose of $\Psi_X(\omega)$. Each eigenvalue $\lambda_i(\omega)$ is proportional to the energy of a certain mode of vibration, whereas each eigenvector $\psi_i(\omega)$ is a mode shape estimate corresponding to given eigenvalue (Yam et al., 2004). The first step of the spectral damage analysis consists in the estimation of the dynamic properties of the structure under investigation, i.e. frequency and damping coefficient. In order to upgrade the spectral analysis and move to higher levels of damage identification, coordinate-dependent parameters must be considered in the procedure. For this purpose, the second step of the method involves the analysis of the complex eigenvectors obtained from the PSD matrix decomposition. Each eigenvector mode shape $\Psi_X(\omega)$ estimation corresponding to a given eigenvalue depends on the nodal coordinates of the system and can provide spatial information concerning the damage. The number of eigenvectors equals the rank of the matrix, or rather the number of independent measured DOFs. The comparison between spectral modes belonging to different scenarios may be used to locate the damage, real eigenvalues are combined with complex eigenvectors through the following expression:

$$\Delta_\Psi = \sum_{j=1}^{n} \left\| \sum_{i=1}^{m} \left[\Psi_j^d(\omega_i) \sqrt{\lambda_j^d(\omega_i)} \right] - \left[\sum_{i=1}^{m} \left[\Psi_j^u(\omega_i) \sqrt{\lambda_j^u(\omega_i)} \right] \right] \right\| \quad (3)$$

where $\Psi(\omega)$ denotes the eigenvector; $\lambda(\omega)$ indicates the corresponding non-zero eigenvalue, m specifies the frequency range, n represents the mode number and upper scripts d and u stand for damaged and undamaged conditions, respectively. Basically, equation (3) reports the quantitative definition of a damage index, which measures the difference between spectral modes belonging to different structural conditions. If only a single damage scenario is available, the index is univocally computed by comparing the DS with the RS; whereas in case of multiple damage scenarios, the index can be calculated either by comparing each DS with the RS (absolute index) or by comparing the current DS with the previous DS (relative index). If the aim is to identify the progressive evolution of damage up to the last scenario, a relative comparison between DSs is more appropriate.

4.2 Application of the spectral damage analysis

The damage analysis over the experimentally induced seven DSs was performed by analysing the direct changes in the modal parameters of the arch as well as the changes in the derivatives of these modal parameters (Masciotta et al., 2016a). As mentioned, from the random impact test data, three square PSD matrices for each scenario were built in MATLAB (2010). Furthermore, two [26×26] matrices from acceleration responses in both normal (z) and tangential (x) direction were also assembled.

In order to define the modal parameters and proceed with the damage analysis, each matrix is then decomposed in eigenvalues and eigenvectors.

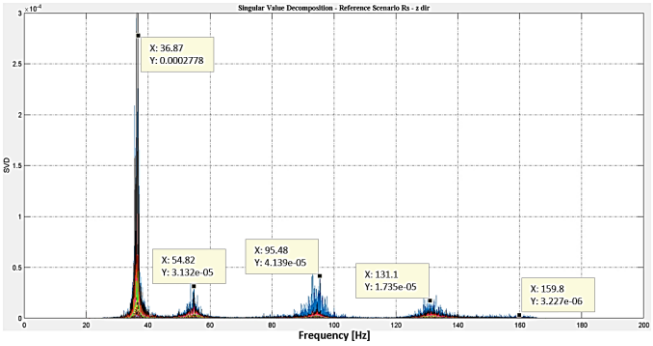

Figure 15. Spectral value decomposition for the random impact excitation.

The eigenvalues decomposition (Figure 15) first performed with regard to the RS and then applied to the seven DSs, allowed to identify the eigenfrequencies to use as qualitative indicators in the damage analysis with global parameters. This type of analysis is essentially based on the observation of shifts in the resonant frequency values. If accurately estimated, direct changes in these modal parameters are proved to be a sensitive indicator of global structural damage.

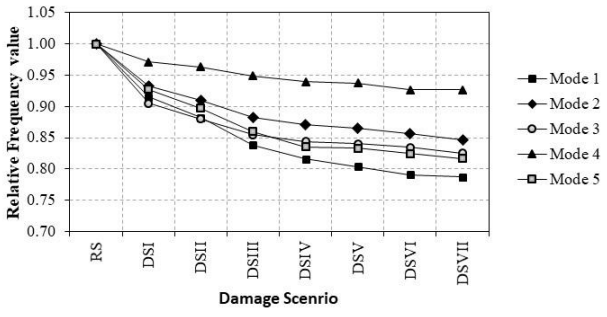

Figure 16. Frequency vs. damage level relationship.

Figure 16 shows the progressive frequency decrease associated to the increasing displacement of the moving abutment. The results confirm a relationship between the level of damage and the relative decrease of the measured frequency, confirming an overall coherence of the experimental results. It is also shown that the higher decrease of the frequency occurs at the first stage of loading, independently on clear evidences of damage represented by the cracks.

The application of the spectral damage analysis described herein involved only the output signal in normal direction.

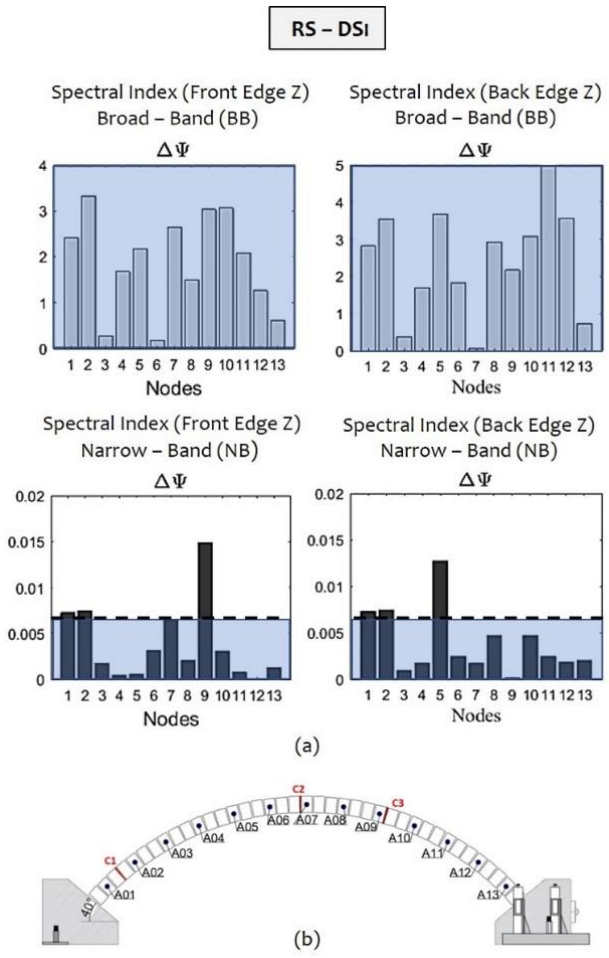

Figure 17. Damage analysis results (RS DS_I) for acceleration responses by BB index (light grey bars) and NB index (dark grey bars)

The results are shown in Figure 17 and 18 for the first and last damage state. In order to evaluate the sensitivity of the algorithm to the considered frequency bandwidth, two types of damage indices are computed and compared:

i) Broad-Band (BB) index;

ii) Narrow-Band (NB) index.

The BB index relies on the difference between spectral modes weighed over the whole frequency domain by the respective on zero singular values. The NB index presented the difference between resonant spectral modes, each one weighed by its relevant eigenvalue at the resonant frequency.

It is worth noting that the bar plots reported in Figure 17 and 18 exhibit as columns as the number of measured Degrees of Freedom (DOFs), while the height of the bar represents an estimate of the intensity of damage at the considered location or a nearby area.

Given this, the review of the results both in the case of the comparative analysis RS vs. DS_I and DS_{VII} respectively confirms the ability of the procedure to highlight the presence of changes in the local features of the arch. Increased values of the index can be associated to the presence of the cracks illustrated in Figure 11, since the values are high particularly at location A01 corresponding the right support, A07 corresponding the key of the arch and the last in the A09.

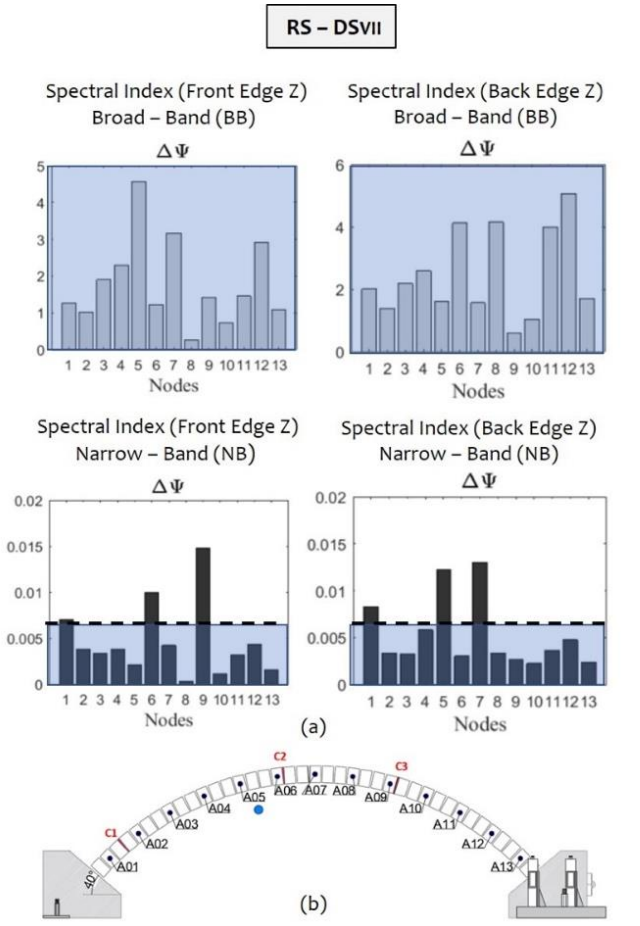

Figure 18. Damage analysis results (RS DS_I) for acceleration responses by BB index (light grey bars) and NB index (dark grey bars)

It is also clear that a certain level of inaccuracy of the procedure is observed as the location A13 is concerned, since low values of the index are provided by the computed data. The motivations of such a result are primarily associated to the proximity of the A13 node to the actuator, whose

vibrations under operational conditions played a negative role in the process.

Furthermore , the results confirm that even at very low displacements like the one associated to DS_I the damage is not negligible and that the crack location is identified by the procedure before that it became visible. A final comment can be devoted to the comparison in terms of performance between BB and NB damage index. Under the described test conditions, NB damage index proved to be more accurate and reliable than the BB index in most of the cases, with regard to the crack sequence.

5 CONCLUSIONS

The present work reported some aspects of an experimental study regarding the ability of spectrum driven damage identification procedures. In particular, the design and development of laboratory tests on masonry arch specimens were discussed. A sequence of static loading and dynamic measurements for modal analysis were performed to collect data to be processed. Despite the complex experimental process, encouraging results were obtained, demonstrating a certain ability of damage detection process to support health stated evaluations of masonry arches. Further work and more detailed analyses are needed to point out critical features of the procedure and define strategies for improving accuracy and reliability.

REFERENCES

Basilio, I., 2007. Strengthening of Arched Masonry Structures with composite materials, *Ph.D Dissertation*, University of Minho, Portugal.

Bentz, E. C., Vecchio, F. J., & Collins, M. P., 2006. Simplified modified compression field theory for calculating shear strength of reinforced concrete elements. *ACI Structural Journal*, *103*(4), 614–624. https://doi.org/10.14359/16438

DIANA, 2018. DIANA Finite Element Analysis, User's Manual - Release 10.2, TNO, Netherlands.

Feenstra, P., 1993. *Computational aspects of biaxial stress in plain and reinforced concrete*. Delft University of Technology,The Netherlands.

Ferreira T.M., Mendes N., Silva R., 2019. Reducing the Seismic Vulnerability of Existing Buildings: Assessment and Retrofit. *Buildings*, 9(6), 148;

Granda, S. & Ferreira, T.M., 2019. Assessing Vulnerability and Fire Risk in Old Urban Areas: Application to the Historical Centre of Guimarães. Fire Technology. 55: 105. https://doi.org/10.1007/s10694-018-0778-z

ICOMOS, 2003. ICOMOS Charter – Principles for the Analysis, Conservation and Structural Restoration of Architectural Heritage. Ratified by the ICOMOS 14th General Assembly in Victoria Falls, Zimbabwe.

Lourenço, P. B., 2002. Computations on historic masonry structures. *Progress in Structural Engineering and Materials*; 4:301–319 (DOI: 10.1002/pse.120).

Lourenço, P. B., 2009. Recent Advances in Masonry Modelling: Micromodelling and Homogenisation. Multiscale *Modeling in Solid Mechanics*, pp. 251-294.

Marra A., Sabino A., Bartolomucci C., Trizio I., Mannella A., Fabbrocino G., 2019. On a Rational and Interdisciplinary Framework for the Safety and Conservation of Historical Centres in Abruzzo Region. *Journal of Architectural Heritage*. https://doi.org/10.1080/15583058.2019.1637478 .

Masciotta, M. G., Ramos, L. F., Lourenço, P. B., Vasta, M., & De Roeck, G., 2016a. A spectrum-driven damage identification technique: Application and validation through the numerical simulation of the Z24 Bridge. *Mechanical Systems and Signal Processing*, *70–71*, 578–600.

Masciotta, M.G., Roque, J.C.A., Ramos, L.F., Lourenço, P.B., 2016b. A multidisciplinary approach to assess the health state of heritage structures: The case study of the Church of Monastery of Jerónimos in Lisbon. *Construction and Building Materials.* Vol. 116, 30. 169-187.

Miranda, F.N. & Ferreira, T.M., 2019. A simplified approach for flood vulnerability assessment of historic sites. *Natural Hazards*, 96: 713.

MATLAB, 2017. MATLAB User's Manual, Release 9.2.0, The Math Works, USA.

Rainieri, C., Fabbrocino, G., Verderame, G.M., 2013. Non-destructive characterization and dynamic identification of a modern heritage building for serviceability seismic analyses. *NDT & E International*, 60, pp. 17-31

Rainieri, C., Marra, A., Rainieri, G.M., Gargaro, D., Pepe, M., and Fabbrocino G., 2015a. Integrated non-destructive assessment of relevant structural elements of an Italian heritage site: the Carthusian monastery of Trisulti. *Journal of Physics: Conference Series* 628.

Rainieri, C., Fabbrocino, G., 2015b. Development and validation of an automated operational modal analysis algorithm for vibration-based monitoring and tensile load estimation. *Mechanical systems and signal processing*, vol. 60-61, p. 512-534, ISSN: 0888-3270.

Ramos, L. F., De Roeck, G., Lourenço, P. B., & Campos-Costa, A., 2010. Damage identification on arched masonry structures using ambient and random impact vibrations. *Engineering Structures*, *32*(1), 146–162. https://doi.org/10.1016/j.engstruct.2009.09.002

SVS, 2018. ARTeMIS Extractor Pro User Manual, Release .5.3.1.1, Structural Vibration Solutions, Aalborg, Denmark.

Wahab, M. A., & De Roeck, G., 1999. Damage detection in bridges using modal curvatures: application to a real damage scenario. *Journal of Sound and Vibration*, *226*(2), 217–235. https://doi.org/10.1006/JSVI.1999.2295